Journal of Hazardous Materials 187 (2011) 241–249

Contents lists available at ScienceDirect

Journal of Hazardous Materials

journal homepage: www.elsevier.com/locate/jhazmat

Polyacrylamide–clinoptilolite/Y-zeolite composites: Characterization and adsorptive features for terbium

Demet Baybaş, Ulvi Ulusoy*

Cumhuriyet University, Department of Chemistry, Sivas 58140, Turkey

ARTICLE INFO

Article history:
Received 6 July 2010
Received in revised form 9 December 2010
Accepted 5 January 2011
Available online 12 January 2011

Keywords:
Adsorption
Zeolite
Lanthanides
Composite
Radiotracer

ABSTRACT

The composites of natural (clinoptilolite) and synthetic zeolite (Z and YZ) with polyacrylamide (PAAm) were synthesized and characterized by FT-IR, TGA, XRD, SEM and PZC analysis. The adsorptive features of the minerals and its composites were investigated for Tb analogues to the rare earth elements (REs) by isotopic tracer method, ^{160}Tb was the radiotracer. The composites were the hybrid formations of PAAm and Z or YZ. Tb adsorption capacities of the composites were higher than those of bare Z and YZ. The compatibility of Tb adsorption kinetics to the second order and Weber–Morris models implied that the sorption process was chemical via ion exchange. The values of enthalpy and entropy changes were positive and the negative free enthalpy change was evidence for the spontaneity of adsorption. The reusability tests for the composites for five uses demonstrated that the adsorbents could be reused after complete recovery of the loaded ion. Unlike PAAm–YZ, PAAm–Z was resistant to acidic environment. The overall results eventually suggested that the composite of Z and PAAm was a potential cost effective adsorbent for Tb^{3+} and REs.

1. Introduction

Chemical precipitation, ion exchange, solvent extraction, reverse osmosis and adsorption are conventionally applied methods for removal and/or recovery of metal ions contributed into aquatic environment by natural or industrial resources. Amongst these, the adsorption is introduced as a favorable one since it has advantages of effectiveness, versatility, simplicity, applicability at very low concentrations, suitability for using batch and continuous processes, ease for operation, little sludge generation, possibility of regeneration and reuse, and low capital cost [1].

In principle, a good adsorbent should have a porous structure (high surface area) and fast adsorption kinetics beside which it should be cost effective. Fly ash, silica gel, zeolite, lignin, seaweed, wool wastes, agricultural wastes, chitin, chitosan, and clay materials are of natural adsorbents comparatively meet these requirements [2,3].

Amongst these, natural zeolites are the most abundant minerals on earth. Clinoptilolite has the highest abundance in comparison to its other common forms: mordenite, phillipsite, chabazite, stilbite, analcime and laumontite. Zeolites are hydrated porous aluminosilicates and possess precious physicochemical features for chemical processes, such as cation exchange, catalysis, molecular sieving and adsorption [4]. Zeolites are also produced synthetically, although they are not economically feasible in large scale applications. They are formed by fusing weighed amounts of feldspar, clay, and soda ash or obtained from mixtures of caustic soda, sodium silicate and bauxite. Natural zeolites generally show low surface area; however, the apparent surface area of some synthetic zeolites can be as high as 700 $m^2 g^{-1}$ [5,6]. Clinoptilolite (Z) and synthetic Y-zeolite (YZ) as the interest of this investigation are classified under the same framework topology encoded with HEU [7].

Although, the usability of Z and YZ in adsorption procedures have been proved with a number of investigations ([8–16] for Z, and [17–23] for Y-zeolite), further researches require for enhancement of adsorptive features and practical usage of zeolites, since the aggregation and coagulation of mineral particles under varying conditions of temperature and electrolytes lead variations in flow properties of these minerals. This is an undesired feature for their practical use as adsorbents since it may result in *e.g.* hydrodynamic constraints in chromatographic and/or column applications.

The use of the mineral as its composite with a polymer may be helpful to overcome these limitations. Besides its practicality, the composition may display more properties of an effective adsorbent than the bare mineral. The result of such composition should be a granular adsorbent similar to conventional ion exchange resins and spherical shape encompasses greater attrition resistance and compression strength [24]. The candidate polymer must be a hydrogel capable of swelling in aquatic solutions, enabling the diffusion

Abbreviations: Z, zeolite (clinoptilolite); YZ, Y-zeolite; PAAm, polyacrylamide.

* Corresponding author. Tel.: +90 346 2191010x1623; fax: +90 346 2191186.
E-mail addresses: ulusoy@cumhuriyet.edu.tr, ulvi.ulusoy@gmail.com (U. Ulusoy).

0304-3894/$ – see front matter © 2011 Elsevier B.V. All rights reserved.
doi:10.1016/j.jhazmat.2011.01.014

and/or transfer of ions towards adsorption sites of the embodied mineral and inert for metal ions.

The aim of this investigation was to introduce the composites of clinoptilolite (Z) and Y-zeolite (YZ) with hydrogel polyacrylamide (PAAm–Z/YZ) for practical use of the zeolites in adsorption procedures. The preparation and characterization of the composites, and its comparative adsorptive features with bare Z and YZ with reference to the dependency on concentrations, time and temperature for Tb^{3+} were investigated by a radiotracer method using ^{160}Tb. Additional consideration was also given to the reusability of the composite.

Tb^{3+} was selected as representative for the entire series of the REs (lanthanides) possessing similar physicochemical features, beside which the advantages of ^{160}Tb are its high natural abundance (100%) and the high cross section for thermal neutron capture ($\sigma = 25.5$ b) of its precursor ^{159}Tb, and the half life of ^{160}Tb (72 days) allows relatively comfortable handling [25]. As the other REs, Tb is also industrially important; it is used in cathode ray tubes, magnets optical computer memories, magnetostrictive alloys, luminescence activator, fluorescence and laser complex [26–28] and catalytic systems [29,30]. Besides the economical interests, the removal/recovery of lanthanides is also important because of its hazardousness in view of toxicity [31,32] and radioactivity in relation to the nuclear wastes [33].

2. Experimental

2.1. Reagents

Zeolite was obtained from Central North Anatolian occurrences associated with Eocene submarine volcanism. The certified (IMO GmbH) chemical composition of zeolite was 71.89% SiO_2, 15.16% Al_2O_3, 6.51% CaO, 1.80% Fe_2O_3, 1.80% MgO, 1.06% Na_2O and 0.59% SrO. The mineral is composed of ~90% zeolite, as clinoptilolite $\{(Na,K)_6{\cdot}[Al_6Si_{30}O_{72}]{\cdot}24H_2O\}$ and mordenite $\{Na_3KCa_2{\cdot}[Al_8Si_{40}O_{96}]{\cdot}28H_2O\}$, 5% quartz, 5% feldspar and smectite in trace level. The ratio of SiO_2/Al_2O_3 is 4.7, which suggests that the mineral is clinoptilolite with reference to the classification of the International Mineralogical Association [7].

Na–Y zeolite (Sigma) was preferred as the synthetic zeolite. The certified composition by the supplier was 63.8% SiO_2, 22.9% Al_2O_3, 13.0% Na_2O, 0.13% Fe_2O_3 and 0.38% CaO. The value of SiO_2/Al_2O_3 was 4.74. The univalent cation exchange capacity (CEC) of zeolite and Y-zeolite determined by ammonium acetate method at pH = 7 [34] were 0.90 mol kg^{-1} and 1.88 mol kg^{-1}.

N,N′-Methylene-bisacrylamide, N,N,N′,N′-tetramethylethylenediamine (TEMED) were purchased from Sigma. Acrylamide monomer, ammoniumperoxodisulfate; APS ($H_8N_2O_8S_2$) and Tb_2O_3 were obtained from Aldrich. All chemicals used were of analytical reagent grade. No pre-treatment was applied to the chemicals, Z and YZ.

2.2. Preparation of composites

PAAm–Z or PAAm–YZ was prepared by direct polymerization of AAm monomer in its related mineral suspensions. The final composition of the composites had 2:1 mass ratio of PAAm to the mineral. APS and TEMED as the initiator and propagator of the polymerization, and N,N′-methylene-bisacrylamide as cross linking agent were used. The composite gels were washed after completion of the polymerization with distilled water until effluent attained water conductivity, dried at ambient temperature, ground and sieved to an average particle size 50 mesh. One batch for each of PAAm–Z or PAAm–YZ was prepared at once to conduct the overall investigation [35].

The composites and its mineral compositions were characterized by FT-IR (Unicam, Mattson-1000), XRD (Shimadzu XRD-6000), SEM (JEOL/JSM-6335F), BET-porosity (Quantachrome, Quantachrome Instruments) and DTG (Shimadzu DT-50) analysis.

Pure PAAm was also prepared for comparison of its swelling features with the composites, Z and YZ. 0.1 g of dried samples were let to swell in water, the swollen samples were then weighed to find swelling ratio with reference to the dry mass.

Since the principal concern of this study was to investigate the adsorptive features of the composites, the bare form of the minerals was only considered for determination of adsorption capacities to find out the effect of the encapsulation in PAAm. The preliminary adsorption investigation for PAAm confirmed that PAAm was inert for Tb^{3+}, as previously proved for Cu^{2+} and Fe^{3+} ions [36].

All experiments were always performed in duplicates for which ±5% was the limit of experimental error. Time to attain equilibration between solution and adsorbent was 24 h. The study temperature was always 298 K unless otherwise stated.

2.3. Preparation of ^{160}Tb tracer

50 mg of Tb_2O_3 was irradiated under a thermal neutron flux of $\approx 10^{13}$ n cm^{-2} s^{-1} in a nuclear reactor (Çekmece Nuclear and Research Centre, Turkey) to obtain ^{160}Tb possessing 1 MBq activity. The irradiated sample was dissolved in 5 mL of 1 M HNO_3, the solution was evaporated near dryness and diluted to provide an activity of 250 Bq mL^{-1}. 1 mL of the tracer stock was used as spike for every 10 mL of Tb solution throughout the investigation.

2.4. Point of zero charge (PZC) and pH dependence of Tb^{3+} adsorption

PZC of the composites and its mineral components was determined with reference to the change in initial and final pH of solutions in presence of 0.1 M of KNO_3 [37]. 0.1 g of each composite or 0.035 g Z and YZ (the equivalent amounts to mineral contents of the composites) were interacted with 10 mL of KNO_3 solutions having a pH in the range of 3–10 for 24 h. 0.1 M of HCl or NaOH were used for the pH adjustments. PZC values were then obtained from the intercepts of the linearity relation between initial pH and ΔpH as the difference between initial and equilibrium pHs ($\Delta pH = pH_e - pH_i$).

For determination of pH effect on Tb adsorption, pH_i of 10 mL 3.1×10^{-3} M (500 mg L^{-1}) Tb^{3+} solutions were adjusted to 1–5.5 beyond which Tb precipitated [38]. The investigation associated with PAAm–YZ was limited with pH = 2.5–5 due to its decomposition at pH lower than 2. 0.1 g fractions of the adsorbents in 10 mL Tb^{3+} solutions were agitated for 24 h at 298 K. The supernatants were separated by centrifugation and the aliquots were taken for the measurements.

Fractional adsorption was determined by gamma-spectrometric method for which a NaI(Tl) detector (combined with a EG&G Ortec multi-channel analyzer and with a software, MAESTRO 32 MCA Emulator, USA) was employed. 5 mL portions of the supernatants and a reference solution (not interacted with the adsorbents) were counted on contact geometry for a time to collect at least 10,000 counts to provide 1% coefficient of variation. The adsorbed fraction of Tb was then derived from the comparison of ^{160}Tb activities at 87, 197, 299, 876, 966 and 1178 keV of the supernatants and those of reference solution.

The same experimental procedure (interaction time, temperature, agitation and centrifugation) and method for Tb determination were applied to the other adsorption studies unless otherwise specified. Tb solutions were prepared from Tb_2O_3 as described in Section 2.3.

2.5. Concentration dependence of adsorption

0.1 g of the composites, YZ and Z were equilibrated with 10 mL Tb^{3+} at concentrations ranging from 1.6×10^{-4} to 1.3×10^{-2} M (25–2000 mg L^{-1}), for which the initial pH was in the range of 5–3.

2.6. Time dependence of adsorption

25 mL fractions of Tb^{3+} solution at 3.1×10^{-3} M (500 mg L^{-1}) were transferred onto the composites (0.5 g of each). 1 mL fractions of solution were withdrawn for 10 h starting immediately after the solution–solid contact and continued with time intervals.

2.7. Temperature dependence of adsorption

Temperature effect on adsorption was studied to reveal the thermodynamic parameters. 0.1 g of the composites was equilibrated with Tb^{3+} solution at 1.6×10^{-3} M (250 mg L^{-1}) at 278, 288, 298, 313 and 323 K.

2.8. Reusability

0.1 g of the composites in polypropylene columns (100 mm height × 10 mm i.d., with a glass-wool over its stopcock) were equilibrated with 10 mL of 1.6×10^{-3} M (250 mg L^{-1}) Tb^{3+} solutions for 2 h (adequate time for completion of the adsorption after kinetic studies). The adsorbed amounts were derived from the contents of solutions at equilibrium. Tb contents of PAAm–Z were eluted with 30 mL of 1 M HCl with a flow rate of 0.5 mL min^{-1} since HCl treatment had no distractive effect on Z [39]. Due to the decomposition of YZ in acidic solutions, 2 M $NaNO_3$ solutions (50 mL) were used for PAAm–YZ [18]. The complete recovery of the adsorbed Tb^{3+} was justified by Tb^{3+} determination in the eluents. The columns were then reconditioned with distilled water until the effluents had a neutral pH. Each sample was subjected to the same procedure for 4 sequential times to provide 5 uses in total.

2.9. Data evaluation

The fractional transfer (F) of ^{160}Tb to solid phase from Tb^{3+} solutions was derived from $F = (A_i - A_e)/A_i$ where A_i and A_e are the activity measured in the reference and equilibrium solutions. The adsorbed amounts (Q (mol kg^{-1})) were then calculated from $Q = [FC_iV/w]$ in which C_i is the initial Tb^{3+} concentration (M), w is the mass of adsorbent (kg) and V is the solution volume (L). Due to the inertness of PAAm, the values of Q were calculated with reference to the Z and YZ content of adsorbents (0.035 g of 0.1 g PAAm–Z/YZ).

The Langmuir and Freundlich models $\{Q = (K_L X_L C_e)/(1 + K_L C_e)$ and $Q = X_F C_e^{\beta}\}$ fitted to the isotherms experimentally obtained, where X_L was the monolayer solution capacity (mol kg^{-1}), K_L was the adsorption equilibrium constant (L mol^{-1}) related to the adsorption energy. X_F and 'β' were empirical Freundlich constants associated with the capacity and intensity of adsorption.

The isotherms were also evaluated with reference to Dubinin–Radushkevich (DR) model to find out the constant (K_{DR} (mol^2 K J^{-2})) related to the sorption energy from $Q = X_{DR} e^{-K_{DR}\varepsilon^2}$ where X_{DR} was sorption capacity (mol kg^{-1}) and ε was Polanyi potential given with $\varepsilon = RT\ln(1 + 1/C_e)$. R and T represented the ideal gas constant (8.314 J mol^{-1} K^{-1}) and absolute temperature (298 K). Free energy change (E (J mol^{-1})) required to transfer 1 mol of ion from the infinity in solution to the solid surface was then derived from $E = (-2K_{DR})^{-1/2}$.

Langmuir isotherms were further considered to predict if the composites were 'favorable' in view of dimensionless factor; $R_D = 1/(1 + K_L C_e)$ and to calculate the mass of composites (W (kg)) for removing half of 100 mg L^{-1} of Tb^{3+} from a hypothetic solution with 'V'(L) volume by $W/V = (C_i - C_e)/[K_L X_L C_e/(1 + K_L C_e)]$ as suggested by Doğan and Alkan [40].

The adsorption kinetics was evaluated with reference to the pseudo-second-order kinetic and intra-particle diffusion (Weber and Morris model) models by $t/Q_t = 1/(kQ_{Mod}^2) + t/Q_{Mod}$ and $Q_t = k_i t^{1/2}$ where Q_t and Q_{Mod} were the adsorbed amounts (mol kg^{-1}) at time t and equilibrium, k and k_i were the rate constants [41]. Initial adsorption rate (H) and the time required for adsorption of half of the concentrations ($t_{1/2}$) was also calculated from $H = kQ_{Mod}^2$ and $t_{1/2} = 1/(kQ_{Mod}) = Q_{Mod}/H$ as described by Ho and McKay [42] and Basha and Murthy [43].

For evaluation of the temperature dependence of adsorption, the distribution coefficients (K_d) were derived from $K_d = Q/C_e$ for each temperature and $\ln K_d$ was depicted against $1/T$ to provide adsorption enthalpy (ΔH (J mol^{-1})) and entropy (ΔS (J mol^{-1} K^{-1})) from the slopes ($\Delta H/R$) and intercepts ($\Delta S/R$) of the depictions with reference to van t'Hoff equation: $\ln K_d = \Delta S/R - \Delta H/(RT)$. Having had ΔH and ΔS, ΔG values were calculated from $\Delta G = \Delta H - T\Delta S$ for 298 K.

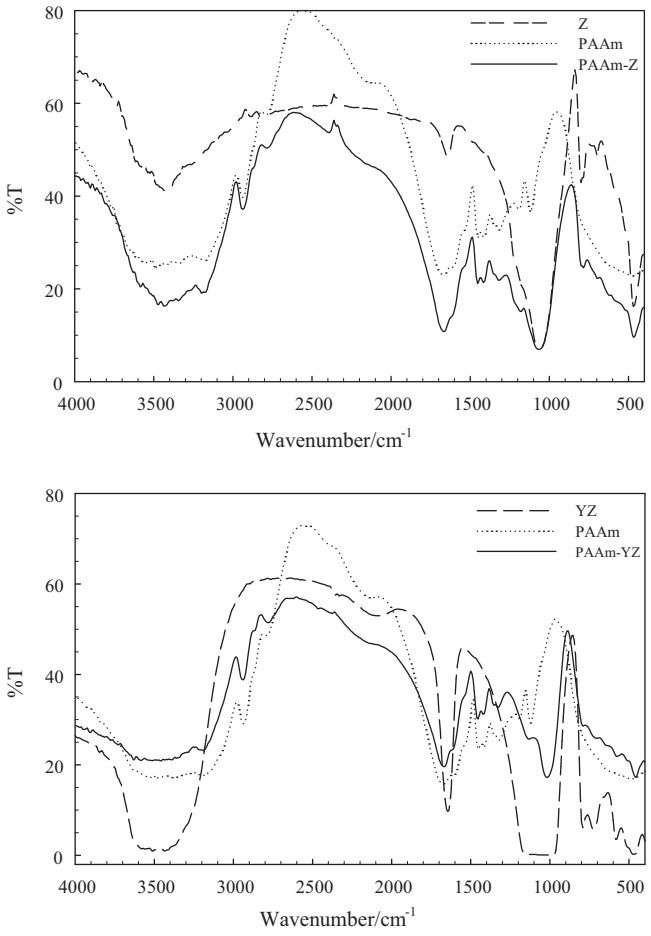

Fig. 1. Comparative IR spectra of the composites and its components.

3. Results and discussion

3.1. Structural evaluation

The FT-IR spectra of the composites and their components were compared in Fig. 1. The appearances of the stretches associated with the crystal lattice of Z (1215 and 1060 cm^{-1} and 800 cm^{-1}) and of YZ (1150–970 cm^{-1}) in PAAm–Z/YZ together with the typical vibra-

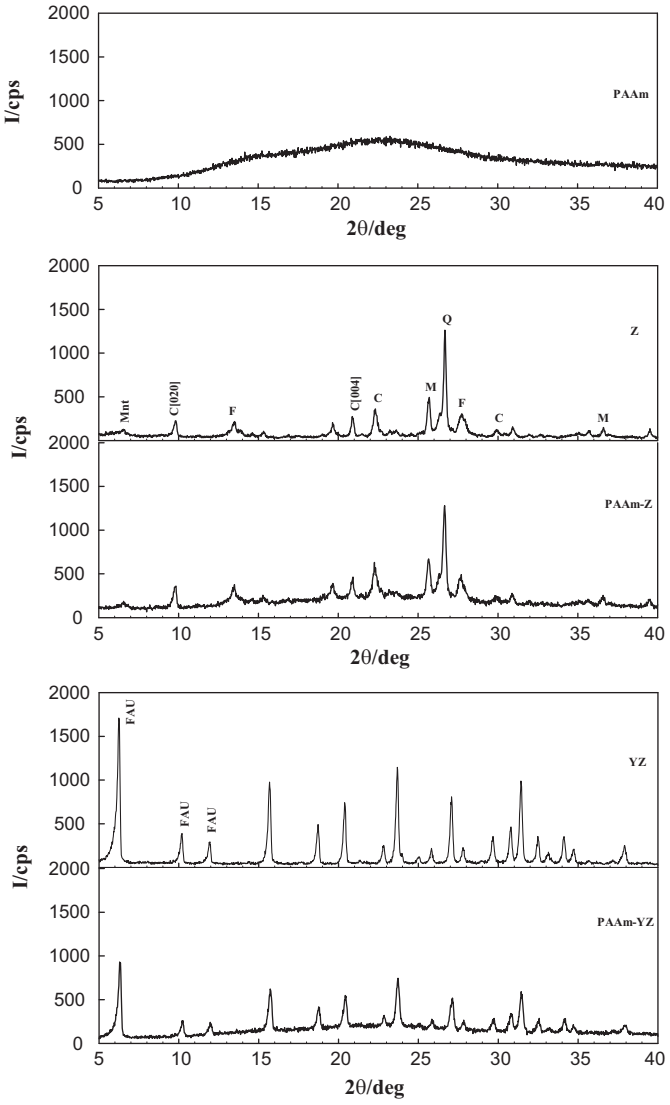

Fig. 2. XRD diffraction patterns [clinoptilolite (C), mordenite (M), montmorillonite (Mnt), kuartz (Q) and feldspar (F) are the main composition of Z, and characteristic reflections defining YZ as faujasite (FAU) type mineral].

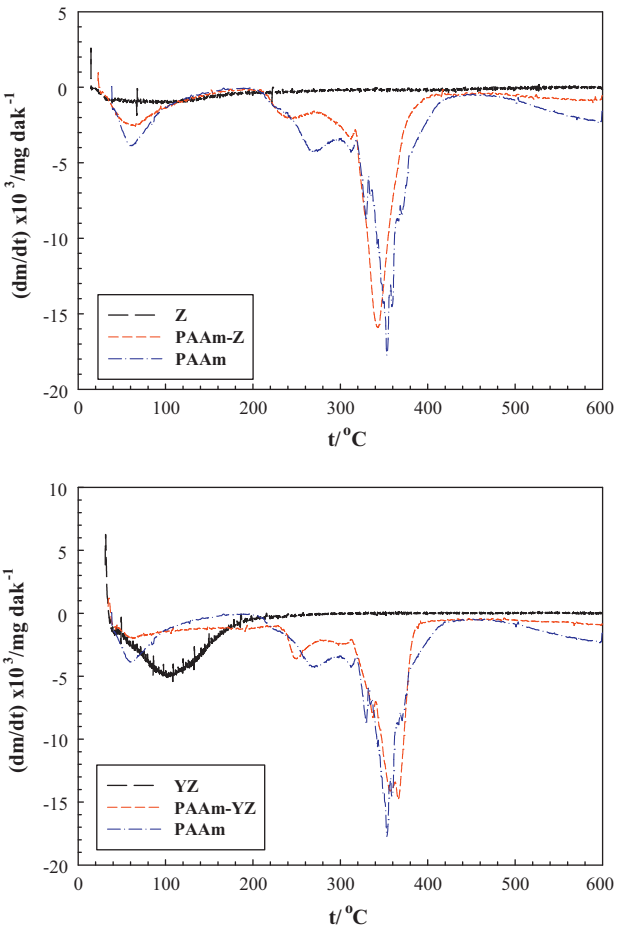

Fig. 3. The derivative TGA curves (heating rate: 10 °C min^{-1} under static air).

tions related to C=O (1650 cm^{-1}), N–H (3490–3185 cm^{-1}, broad band), C–H (2940 and 1455 cm^{-1}) terminals of PAAm [8,44–48] were of evidences for the hybrid formation of the composites.

Pure PAAm had a typical noncrystalline (amorphous) pattern, while the composites had the typical crystallite reflections associated with the mineral components (Fig. 2). Clinoptilolite was characterized with the diffractions appeared at 9.8 and 22.3 ($2\theta^{\circ}$) representing d_{020} and d_{004} reflections beside the others [8,49–51].

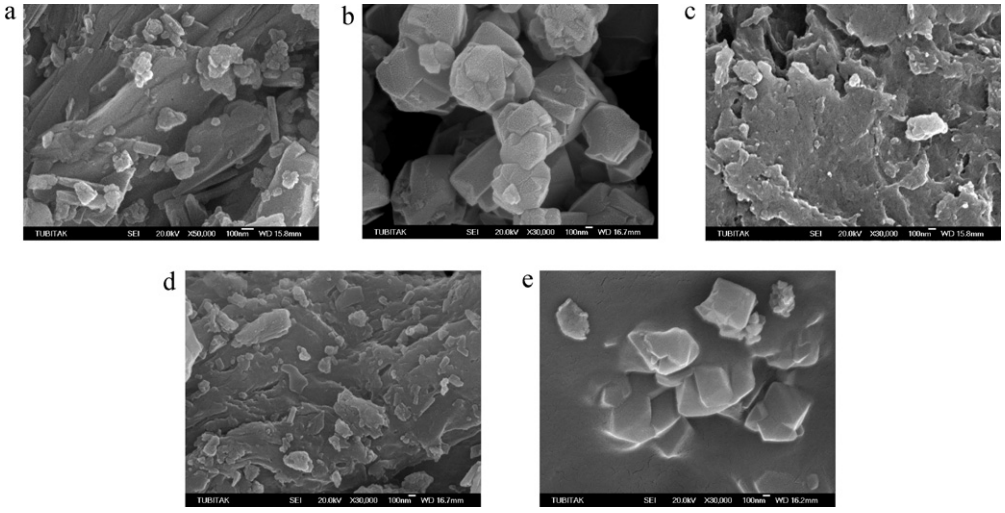

Fig. 4. SEM views of Z (a), YZ (b), PAAm (c), PAAm–Z (d) and PAAm–YZ (e).

Table 1
Derivative TGA analysis.

Material	Loss of mass (% (w/w))			
	25–100 °C	100–200 °C	200–400 °C	400–600 °C
PAAm	9.2	2.6	59.2 (353)[a]	37.6
Z	3.3	3.4	2.5	0.8
PAAm–Z	7.2	3.1	46.0 (342)	13.4
YZ	9.2	13.7	1.2	–
PAAm–YZ	5.2	6.7	48.6 (337)	18.4

[a] Temperatures at which the maximum mass losses were observed.

Y–zeolite was a faujasite type mineral defined by the reflections at 6.3, 10.3 and 12.1 ($2\theta^{\circ}$) [5,21,22,48,49]. Bare minerals and the composites had similar XRD patterns; there were not any distortions and shifts in any of the peaks, which predicated that the minerals were not deformed with inclusion of the hydrogel. The crystallite sizes (S (nm)) were derived from Scherer's formula: $S = 0.9K_{\alpha}/(\mathrm{FWHM}\cos\theta)$, where K_{α} was the wavelength of X-ray beam (0.15406 nm), FWHM was the full width at half maximum (rad) of the considered θ angle with reference to the observed reflections with relative intensity higher than 10%. The mean of sizes and its S.E.M. were 380 ± 27 nm for Z and 314 ± 18 nm for PAAm–Z ($n = 8$), and 440 ± 8 nm for YZ and 339 ± 8 nm for PAAm–YZ ($n = 15$) indicating a significant diminish ($p < 0.05$) in crystallite sizes for both Z (-67 ± 13 nm) and for YZ (-101 ± 8 nm) in the corresponding composites. This should be an evidence for the fine dispersion of mineral particles in PAAm and suggest that the adsorption capacities of the composites should be higher than the bare minerals due to the increase in surface area as a catalyzing factor for the adsorption.

The derivative TGA curves and the observed mass losses within the defined range of temperature (Fig. 3 and Table 1) showed that the mineral components had a few percent mass losses mainly associated with its water contents. The loss at 50–200 °C was due to weakly bound water and that at 200–400 °C was related to the water located in zeolite cavities and bound to the framework cations [15]. Beside the small mass loss indicating removal of moisture up to 200 °C, the characteristic peaks in PAAm and its composites were observed. As suggested by Van Dyke and Kasperski [52], these were associated with the thermal degradation of PAAm realized in three steps: the emissions of H_2O, CO_2 and NH_3 after decomposition of pendant amide groups at 220–340 °C, the losses of H_2O, CO_2, imides and nitriles after the main chain breakdown at 340–440 °C, and the releases during carbonization of the polymer at 440–600 °C. The temperatures at maximum mass losses observed were 353 °C for PAAm, 342 °C for PAAm–Z and 337 °C for PAAm–YZ. The slight decrease observed for PAAm in the composites was attributed to the catalytic effect of mineral components by a higher heat transfer to PAAm.

SEM views of the composite and its components (Fig. 4) substantiated the obvious change in the morphology of the minerals by introduction of PAAm. The crystallite appearances of the minerals changed to be amorphous impressions (plated crystallites) in the composites. This should also be of evidences for the hybrid formation of the composites from its components.

All the studied materials had microporosity with reference to the IUPAC classification, since their pore diameter values were <2 nm [53] (Table 2). Although the encapsulation of Z and YZ in PAAm significantly decreased the BET values and pore volume of the minerals, the changes in these values were not effective factors on the adsorption (see Section 3.3) since PAAm was inert for Tb^{3+} adsorption.

The swelling study showed that the swelling of the composites and PAAm was completed in a very short time (≈2 min). The swelling ratios were 1240% for PAAm, 150% and 1275% for Z and PAAm–Z, and 125% and 1300% for YZ and PAAm–YZ. By considering the PAAm contents of the composites (66% of total mass), it was seen that the involvement of Z or YZ in PAAm significantly increased water imbibing capacities of the composites in comparison to that of pure PAAm. This was explained by the cross-linking efficiency in preparation of PAAm and the composites, i.e., the hydrogel containing the more crosslinking agent (N,N′-methylenebisacrylamide) had the lower swelling [54]. Here, the presence of minerals in preparation of the composites decreased the efficiency of crosslink formations so that the composites had higher water imbibing capacities than the more densely crosslinked PAAm.

Table 2
Physical characteristics.

	BET ($m^2\ g^{-1}$)	Average pore volume ($cm^3\ g^{-1}$)	Average pore diameter (nm)
PAAm	3.5	0.02	0.22
Z	10.4	0.07	0.44
PAAm–Z	2.7	0.03	0.77
YZ	946	1.57	0.44
PAAm–YZ	35.7	0.10	0.44

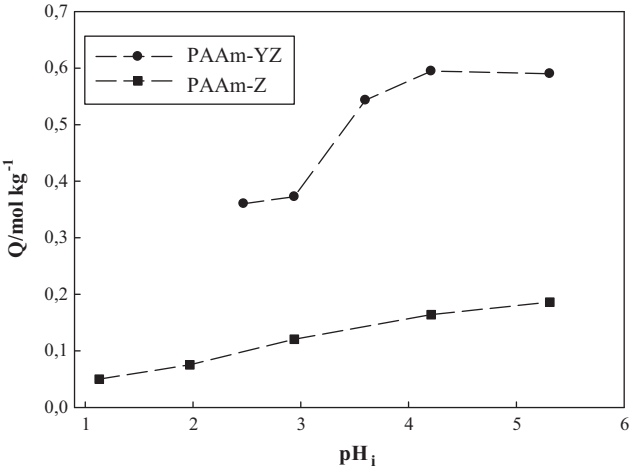

Fig. 5. The effect solution pH on Tb^{3+} adsorption onto the composites.

3.2. pH dependence of adsorption and PZC

The amounts adsorbed onto the composites increased with increasing pH (from 0.05 mol kg^{-1} to 0.19 mol kg^{-1} for PAAm–Z and from 0.36 mol kg^{-1} to 0.55 mol kg^{-1} for PAAm–YZ) and reached a plateau around pH = 3.5 for PAAm–YZ (Fig. 5). The values of adsorbed amounts at pH = 3–4 were close to the maximum adsorption capacities of the composites (see Section 3.3). The pH dependence of adsorption suggested that Tb^{3+} ions were adsorbed via ion-exchange mechanism and the pH solution influenced the adsorption due to the competition of Tb^{3+} and hydrogen ions. As the pH level increased the concentration of the hydrogen ions decreased so that the amounts of adsorbed Tb^{3+} ions increased [10]. The ΔpH ($\Delta pH = pH_i - pH_e$) values were always $\Delta pH > 0$ which were predicative for the basic contribution of the adsorption (Table 3).

The values of point of zero charge (PZC; isoelectric point, the pH of solutions at which the surface of the adsorbents have zero charge) were derived from the intercepts of the linear relations ($p < 0.05$) between ΔpH and pH_i (Fig. 6). The values of PZC were 7.9 for Z, 7.3 for PAAm–Z, 7.8 for YZ and 6.4 for PAAm–YZ so that the PZC of minerals slightly shifted to acidity after its entrapment in PAAm. This also emphasized that the use of minerals in the com-

Table 3
pH dependence of Tb^{3+} adsorption.

PAAm–Z			PAAm–YZ		
pH_i	ΔpH[a]	Q (mol kg^{-1})	pH_i	ΔpH	Q (mol kg^{-1})
1.1	1.0	0.05	2.5	1.8	0.36
2.0	1.0	0.08	2.9	1.3	0.37
2.9	2.7	0.12	3.6	1.5	0.54
4.2	1.7	0.16	4.2	1.2	0.59
5.3	0.7	0.19	5.3	0.6	0.55

[a] $\Delta pH = pH_e - pH_i$.

posite forms enhanced the adsorptive features in view of PZC, i.e., the number of adsorptive sites increased at lower pHs.

At the PZC, the surface of aluminosilicates had amphoteric ≡SOH sites in aquatic solutions and they were either protonated to form $\equiv SOH_2^+$ or deprotonated to form $\equiv SO^-$, i.e., the $\equiv SO^-$ concentration increased with increasing pH whereas ≡SOH concentration decreased with increasing pH [55]. The higher acidity caused the higher repulsion for the positively charged Tb^{3+} ions. Thus the adsorption increased with increasing pH.

By considering the values of PZC and pH dependence of adsorption together with mononuclear Tb^{3+} species [$Tb(OH)^{2+}$ and $Tb(OH)_2^+$] reported by Rönnback et al. [56] and Migdisov et al. [57], the following adsorption mechanisms were envisaged. Mechanisms (2) and (3) should be the explanation of the increase in ΔpH after the adsorption (Table 3).

$$3(\equiv SO^-) + Tb^{3+} \rightleftarrows (\equiv SO)_3Tb \quad (1)$$

$$3(\equiv SO^-) + Tb(OH)^{2+} \rightleftarrows (\equiv SO)_3Tb + OH^- \quad (2)$$

$$3(\equiv SO^-) + Tb(OH)_2^+ \rightleftarrows (\equiv SO)_3Tb + 2OH^- \quad (3)$$

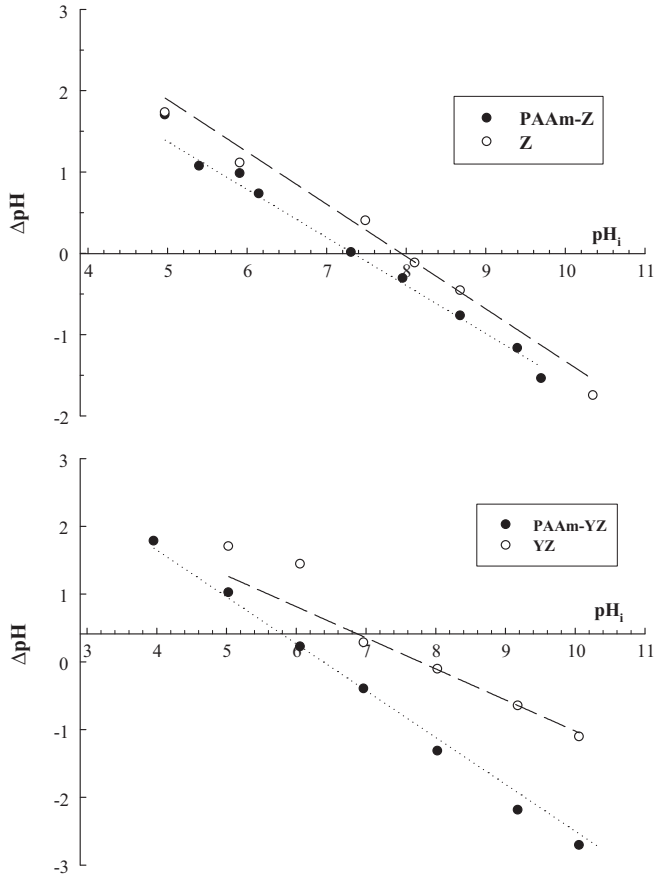

Fig. 6. Comparative PZC plots.

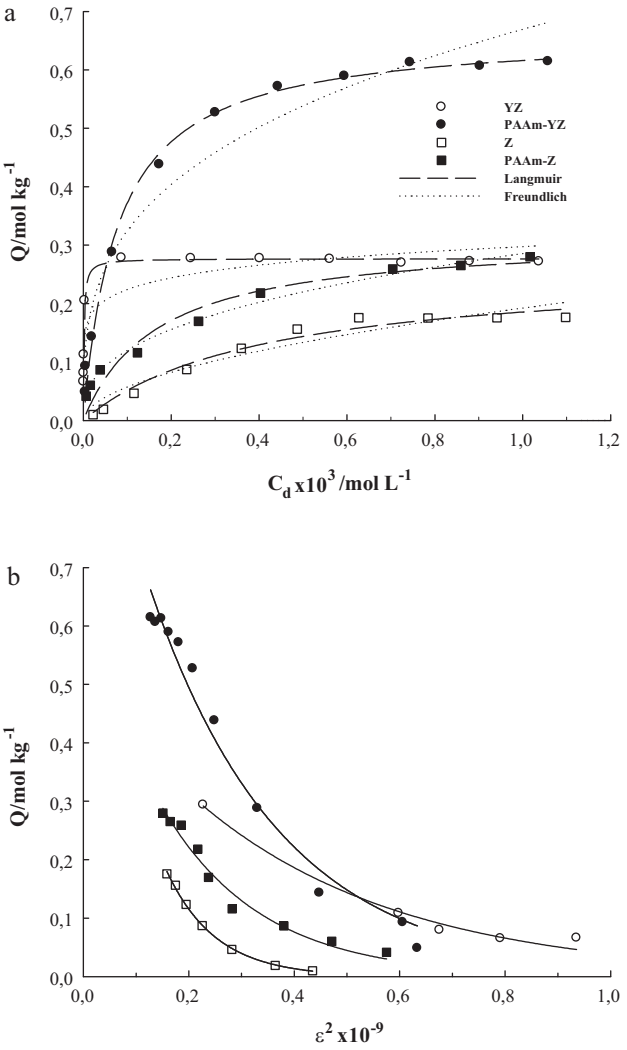

Fig. 7. Compatibility of experimentally obtained adsorption isotherms to Langmuir and Freundlich models.

Because of its relevance to the reusability of the composites (see below); mechanisms (4)–(7) were additionally proposed for the recovery and reconditioning procedures.

$$(\equiv SO^-)_3Tb + 3H^+ \rightleftarrows 3(\equiv SOH) + Tb^{3+} \quad (4)$$

$$\equiv SOH + H^+ \rightleftarrows \equiv SOH_2^+ \quad (5)$$

$$\equiv SOH_2^+ + H_2O \rightleftarrows \equiv SOH + H_3O^+ \quad (6)$$

$$\equiv SOH + H_2O \rightleftarrows \equiv SO^- + H_3O^+ \quad (7)$$

3.3. Concentration dependence of adsorption

The profiles of adsorption isotherms were 'L' or 'H' types of Giles classification [58] (Fig. 7 and Table 4), in which 4 particular cases are commonly used as the 4 main types (C, L, H and S). The 'L' and 'H' types are observed for substrate having high affinity to the adsorbent. The 'L' type means that the ratio between the concentrations of the substrate remaining in solution and adsorbed on the solid decreases with the increasing substrate concentration providing a concave reaching to an asymptotic plateau referring the monolayer adsorption capacity; X_L. The 'H' type is a particular case of the 'L' isotherm, where the initial slope is very high [59].

Both YZ and PAAm–YZ had higher adsorption capacity than Z and PAAm–Z because of the considerable difference between CEC

Table 4
Parameters for Tb^{3+} adsorption derived from Langmuir, Freundlich and DR models.

	YZ	PAAm–YZ	Z	PAAm–Z
Langmuir				
X_L (mol kg^{-1})	0.28	0.66	0.26	0.32
K_L (L mol^{-1})	66,070	1270	240	594
R^2	0.974	0.992	0.976	0.946
Freundlich				
X_F	0.52	2.84	2.18	1.62
β	0.12	0.31	0.53	0.38
R^2	0.819	0.950	0.928	0.992
DR				
X_{DR} (mol kg^{-1})	0.38	1.11	0.69	0.53
$-K_{DR} \times 10^9$ (mol^2 KJ^{-2})	1.4	4.0	9.2	5.0
R^2	0.880	0.978	0.991	0.988
E (kJ mol^{-1})	10.2	11.2	7.4	10.0

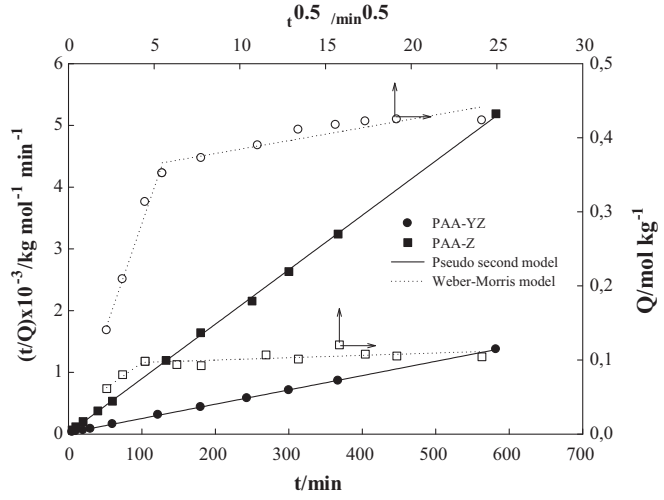

Fig. 8. Fitting of Tb^{3+} adsorption kinetics to the pseudo second order (t/Q_t vs. t) and Weber–Morris (Q_t vs. $t^{0.5}$) models.

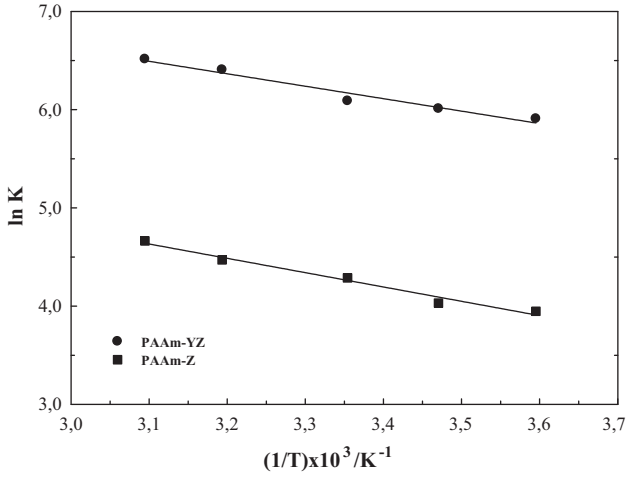

Fig. 9. Temperature dependence of adsorption.

Table 6
Thermodynamic parameters for Tb^{3+} adsorption onto the composites.

	ΔH (kJ mol^{-1})	ΔS (J mol^{-1} K^{-1})	$-\Delta G$ (kJ mol^{-1})	R^2
PAAm–YZ	10.5	87	15.4	0.964
PAAm–Z	12.1	76	10.5	0.980

Table 7
Reusability of the composites for Tb^{3+} adsorption from 1.57×10^{-3} M (250 mg mL^{-1}) Tb^{3+} solutions (the regeneration eluents were 2 M $NaNO_3$ for PAAm–YZ and 1 M HCl for PAAm–Z).

Reuse no.	PAAm–YZ	PAAm–Z
1	66.1 (100)[a]	29.3 (100)
2	67.5 (102)	31.4 (107)
3	65.2 (99)	31.2 (106)
4	61.5 (93)	31.6 (108)
5	63.3 (96)	32.9 (112)
Mean ± S.E.M.	64.7 ± 2.3 (98 ± 4)	31.3 ± 1.3 (107 ± 4)

[a] Percentage adsorption with reference to the first use assumed to be 100%.

values of YZ and Z. The X_L values of the composites (especially PAAm–YZ) were higher than the bare form of mineral components indicating that the encapsulation of YZ and Z in PAAm increased the adsorption of Tb. The increase in adsorption was attributed to catalytic contribution of PAAm to the adsorption process; the fine dispersion of mineral particles in PAAm caused the expansion of adsorptive surfaces and increased the available sites for adsorption. These results signified that the use of YZ and Z in the form of composites was an advantage for removal of Tb^{3+} ions especially by PAAm–YZ, but not for the recovery procedure by acidic solutions in which YZ was chemically instable [18].

$E_{DR} \cong 8$–16 kJ mol^{-1} is assumed as the energy range for definition of the nature of adsorption; the process is ion exchange if E_{DR} is in this interval, chemisorptions are effective driving force if E_{DR} was higher than 16 kJ mol^{-1} [60,61]. The E_{DR} values of this investigation suggested that the adsorption process took place via ion exchange. The energy required for adsorption to the composites was higher than those for adsorption to bare minerals.

The values of 'R' found from dimensionless analysis were always $0 < R < 1$, i.e., the adsorbents were favorable for Tb^{3+} adsorption. The mass of adsorbents for removal of 50% of Tb from a hypothetical solution containing 100 mg L^{-1} Tb^{3+} were 3 and 12 g L^{-1} for YZ and PAAm–YZ, and 17 and 4 g L^{-1} for Z and PAAm–Z. The sufficiency of such low amounts for Tb removal/recovery procedures should ascertain the cost effectiveness of PAAm–Z in comparison to PAAm–YZ, since Z is naturally occurring highly abundant mineral, resistant to acidic and basic solutions, and reusable unlike 'YZ' (see below).

3.4. Time dependence of adsorption

The compatibility of Tb^{3+} adsorption kinetics to the pseudo-second order and intra-particle diffusion (Weber–Morris) models were presented in Fig. 8 and Table 5.

The statistical significance of coefficients of regressions ($p < 0.05$) indicated that the second order model was the best defining kinetic model for adsorption of metal ion in aquatic mediums [42]. This was also consistent with closeness of the Q values at equi-

Table 5
Kinetic parameters for Tb^{3+} adsorption onto the composites.

	Pseudo second-order model						Weber–Morris model	
	k (mol^{-1} kg min^{-1})	Q_{Mod} (mol kg^{-1})	Q_e (mol kg^{-1})	$H \times 10^2$ (mol kg^{-1} min^{-1})	$t_{1/2}$ (min)	R^2	$k_i \times 10^3$ (mol kg^{-1} min$^{0.5}$)	R^2
PAAm–YZ	0.25	0.43	0.40	4.70	9.2	0.999	4.06	0.832
PAAm–Z	4.84	0.11	0.11	6.18	1.8	0.999	1.07	0.693

Table 8
Lanthanide adsorption by different adsorbents.

Adsorbent	RE (III)	Q (mol kg^{-1})	Reference
XAD-4 chelating resin containing bicine ligands	La, Nd, Tb	0.42, 0.25, 0.38	[63]
2-Thenoyltrifluoroacetone supported onto polyurethane foam	Tb	0.042	[64]
A resin with bis(2,4,4-trimethylpentyl) monothiophosphinic acid	Tm	0.50	[65]
N,N′-Dimethyl-N,N′-dibutyl tetradecyl malonamide coated magnetic particles	Eu	0.36	[66]
Algaes (*Undaria pinnatifida* and *Sargassum hemiphyllum*)	La	$4.6–5.0 \times 10^{-6}$	[67]
Hydroxyapatite	Tb-ligand	0.10	[25]
Saccharomyces cerevisiae microorganisms	Nd	0.08	[68]
Atapulgite	Eu	3×10^{-6}	[69]
Z and PAAm–Z	Tb	0.26 and 0.32	This study
YZ and PAAm–YZ	Tb	0.28 and 0.66	This study

librium obtained from the model (Q_{Mod}) and experiments (Q_e). The well compatibility also confirms the Langmuir model; the overall adsorption rate (differential change in the surface occupied by solid, θ_t, with the time, t) is the difference between adsorption and desorption rates, $d\theta_t/dt = k_a C_e(1-\theta_t) - k_d\theta_t$ where $\theta_t = Q_t/X_L$ (Q_t and X_L are the amounts adsorbed at time t and the Langmuir maximum adsorption capacity) [62].

The depictions of Q_t as a function of $t^{0.5}$ (Weber–Morris model) were not provided intercepts at origin defining the adsorption process controlled by diffusion but it was a curve that could be evaluated in two linear parts [40]: the one with steep rise associated with the initial rapid uptake under the boundary layer effects and the other with slow rise related to the intraparticle diffusion after the completion of external coverage. This was also suggested that the overall adsorption process was concentration dependent, i.e., the nature of adsorption chemical via complex formation and/or ion exchange.

The rate constants implied that the faster adsorption was in favor of PAAm–Z in comparison to PAAm–YZ for which the half lives (9.2 min for PAAm–YZ and 1.8 min for PAAm–Z) were of evidences. These findings also proved the advantage of using natural zeolite instead of YZ for adsorption of Tb^{3+}.

3.5. Temperature dependence of adsorption

The thermodynamic parameters derived from the depictions of $1/T$ as a function of '$\ln K_d$' (Fig. 9) were introduced in Table 6.

The enthalpy and entropy changes were ΔH and $\Delta S > 0$ for both composites, i.e., the overall process was endothermic and the randomness in the solid–solution interface increased along with the adsorption process. Here, the enthalpy change is also related to the Langmuir approach defining K_L by $K_L = A(E_a^{desorption} - E_a^{adsorption})/RT = Ae^{-\Delta H/RT}$ where 'A' and 'E_a' are the frequency factor and the activation energy [70].

Gibbs free enthalpy change was $\Delta G < 0$ indicating that the adsorption process was spontaneous.

3.6. Reusability

The reusability features indicated that the means and its ±S.E.M. of the percentage adsorption obtained from the four following uses after the first were 64.7 ± 2.3% for PAAm–YZ and 31.3 ± 1.3% for PAAm–Z (Table 7). The values of means were not significantly different from the values of their first use; 66.1% and 29.3% assumed to be 100% ($p < 0.05$). The IR spectra obtained before and after reuses provided no evidence signifying any changes in the structures. Storage foregoing had also no effect on the structural stability.

The sorption capacities of the composites and the bare minerals for Tb were compared with other adsorbents reported literature in Table 8. The comparison obviously showed that PAAm–Z should be considered amongst the favorite adsorbents besides its reusability and cost effectiveness.

4. Conclusion

Polyacrylamide–Z/YZ composites were synthesized and characterized by FT-IR, TGA, XRD, SEM and PZC analysis. The adsorptive features of the minerals and its composites were investigated for Tb analogues to the rare earth elements by isotopic tracer method, ^{160}Tb was the tracer.

The composites had the features substantially different from its polymer and mineral components. Tb adsorption capacities of the composites were higher than those of bare Z and YZ.

The compatibility of Tb adsorption kinetics to the second order and intraparticle diffusion models implied that the rate controlling step was concentration dependent i.e., the sorption process was chemical (ion exchange) that followed by intraparticle diffusion.

The values of enthalpy and entropy changes were positive, and the negative free enthalpy change was evidence for the spontaneity of adsorption. The chemical nature of Tb adsorption was consistent with both thermodynamic parameters and the free energy changed obtained from DR model.

The reusability of both composites for five uses demonstrated that the adsorbents could be reused after complete recovery of the loaded ion. Unlike PAAm–YZ, PAAm–Z was resistant to acidic environment.

Acknowledgment

This work was supported by The Research Fund of Cumhuriyet University (CÜBAP) to which the authors are grateful.

References

[1] K.G. Bhattacharyya, S.S. Gupta, Adsorption of a few heavy metals on natural and modified kaolinite and montmorillonite: a review, Adv. Colloid Interface Sci. 140 (2008) 114–131.
[2] A. Demirbas, Heavy metal adsorption onto agro-based waste materials: a review, J. Hazard. Mater. 157 (2008) 220–229.
[3] F.C. Wu, R.L. Tseng, R.S. Juang, A review and experimental verification of using chitosan and its derivatives as adsorbents for selected heavy metals, J. Environ. Manage. 91 (2010) 798–806.
[4] S. Wang, Y. Peng, Natural zeolites as effective adsorbents in water and wastewater treatment, Chem. Eng. J. 156 (2010) 11–24.
[5] H. Faghihian, N. Godazandeha, Synthesis of nano crystalline zeolite Y from bentonite, J. Porous Mater. 16 (2009) 331–335.
[6] V.K. Gupta, P.J.M. Carrott, M.M.L. Ribeiro Carrott, Suhas, Low-cost adsorbents: growing approach to wastewater treatment—a review, Crit. Rev. Environ. Sci. Technol. 39 (2009) 783–842.
[7] Ath. Godelitsas, Th. Armbruster, HEU-type zeolites modified by transition elements and lead, Micropor. Mesopor. Mater. 61 (2003) 3–24.
[8] W. Mozgawa, The influence of some heavy metals cations on the FTIR spectra of zeolites, Mol. Struct. 555 (2000) 299–304.
[9] S. Wang, E. Ariyanto, Competitive adsorption of malachite green and Pb ions on natural zeolite, J. Colloid Interface Sci. 314 (2007) 25–31.
[10] S. Wang, T. Terdkiatburana, M.O. Tadé, Adsorption of Cu(II), Pb(II) and humic acid on natural zeolite tuff in single and binary systems, Sep. Purif. Technol. 62 (2008) 64–70.
[11] I. Rodriguez-Iznaga, A. Gomez, A. Rodriguez-Fuentes, A. Benitez-Aguilar, J. Serrano-Ballan, Natural clinoptilolite as an exchanger of Ni^{2+} and NH_4^+ ions under hydrothermal conditions and high ammonia concentration, Micropor. Mesopor. Mater. 53 (2002) 71–80.

[12] M. Panayotova, B. Velikov, Kinetics of heavy metal ions removal by use of natural zeolite, J. Environ. Sci. Health, Part A: Toxicol./Hazard. Subst. Environ. Eng. 37 (2002) 139–147.
[13] M.K. Doula, A. Ioannou, The effect of electrolyte anion on Cu adsorption–desorption by clinoptilolite, Micropor. Mesopor. Mater. 58 (2003) 115–130.
[14] A. Top, S. Ülkü, Silver, zinc, and copper exchange in a Na–clinoptilolite and resulting effect on antibacterial activity, Appl. Clay Sci. 27 (2004) 13–19.
[15] P. Castaldi, L. Santona, C. Cozza, V. Giuliano, C. Abbruzzese, V. Nastro, P. Melis, Thermal and spectroscopic studies of zeolites exchanged with metal cations, J. Mol. Struct. 734 (2005) 99–105.
[16] M.E. Argun, Use of clinoptilolite for the removal of nickel ions from water: kinetics and thermodynamics, J. Hazard. Mater. 150 (2008) 587–595.
[17] M.E.D.G. Azenha, M. da Graça Miguel, S.J. Formosinho, H.D. Burrows, The characterization by luminescence spectroscopy of uranium (VI) incorporated into zeolites and aluminas, J. Mol. Struct. 563–564 (2001) 439–442.
[18] J.S. Kim, M.A. Keane, The removal of iron and cobalt from aqueous solutions by ion exchange with Na–Y zeolite: batch, semi-batch and continuous operation, J. Chem. Technol. Biotechnol. 77 (2002) 633–640.
[19] M.A.S.D. Barros, A.S. Zola, P.A. Arroyo, E.F. Sousa-Aguiar, C.R.G. Tavares, Binary ion exchange of metal ions in Y and Z zeolites, Braz. J. Chem. Eng. 20 (2003) 413–421.
[20] B. Thomas, S. Sugunan, Dehydration of aldoximes on rare earth exchanged (La^{3+}, Ce^{3+}, Re^{3+}, Sm^{3+}) Na–Y zeolites: a facile route for the synthesis of nitriles, J. Porous Mater. 14 (2007) 471–480.
[21] N.N. Fathima, R. Aravindhan, J.R. Rao, B.U. Nair, Dye house wastewater treatment through advanced oxidation process using Cu-exchanged Y zeolite: a heterogeneous catalytic approach, Chemosphere 70 (2008) 1146–1151.
[22] Z.Y. Zhang, T.B. Shi, C.Z. Jia, W.J. Ji, Y. Chen, M.Y. He, Adsorptive removal of aromatic organosulfur compounds over the modified Na–Y zeolites, Appl. Catal. B 82 (2008) 1–10.
[23] J. Wang, F. Xu, F. Xie, Z. Mei, Q. Zhang, J. Cai, W. Cai, The enhanced adsorption of dibenzothiophene onto cerium/nickel-exchanged zeolite Y, J. Hazard. Mater. 163 (2009) 538–543.
[24] A. Tayyebi, A. Khanchi, M.B. Ghofrani, M. Outokesh, Synthesis and characterization of a bentonite–alginate microspherical adsorbent for removal of uranyl ions from aqueous solutions, Sep. Sci. Technol. 45 (2010) 288–298.
[25] C. Rill, Z.I. Kolar, G. Kickelbick, H.Th. Wolterbeek, J.A. Peters, Kinetics and thermodynamics of adsorption on hydroxyapatite of the [^{160}Tb] terbium complexes of the bone-targeting ligands DOTP and BPPED, Langmuir 25 (2009) 2294–2301.
[26] W. Yin, M. Chen, T. Lu, M. Akashi, X. Huang, Study on interaction between Tb(III) and poly(N-isopropylacrylamide), Eur. Polym. J. 42 (2006) 1305–1312.
[27] X. Chen, B. Yan, Induced synthesis of ZnO:Tb^{3+} green hybrid phosphors by the assembly of polyethylene glycol matrices, Mater. Lett. 61 (2007) 1707–1710.
[28] A.K. Singh, P. Singh, S. Banerjee, S. Mehtab, Development of electrochemical sensors for nano scale Tb(III) ion determination based on pendant macrocyclic ligands, Anal. Chim. Acta 633 (2009) 109–118.
[29] J. Fahy, D.L. Trimma, D.J. Cookson, Four component catalysis for the hydroalkylation of benzene to cyclohexyl benzene, Appl. Catal. A 211 (2001) 259–268.
[30] H. Yahiro, T. Nagano, H. Yamaura, Direct decomposition of nitrogen monoxide over Cu-MFI containing rare-earth elements: Sm and Gd as promoter, Catal. Today 126 (2007) 284–289.
[31] S. Hirano, K.T. Suzuki, Exposure, metabolism, and toxicity of rare earths and related compounds, Environ. Health Perspect. 104 (1996) 85–95.
[32] U. Ulusoy, J.E. Whitley, Profiles of faecal output of rare earth elements and stable isotopic tracers of iron and zinc after oral administration, Br. J. Nutr. 84 (2000) 605–617.
[33] R.G. Whymer, Reprocessing of nuclear fuel, in: G.R. Chopin, M.Kh. Khankhasayev (Eds.), Chemical Separation Technologies and Related Methods of Nuclear Waste Management, Kluwer Academic Publishers, Netherlands, 1998, pp. 29–52.
[34] H.D. Chapman, Cation-exchange capacity, in: C.A. Black (Ed.), Methods of Soil Analysis – Chemical and Microbiological Properties. Agronomy 9, Am. Soc. Agro. Inc., Madison, WI, 1965, pp. 891–901.
[35] U. Ulusoy, S. Şimşek, Ö. Ceyhan, Investigation for modification of polyacrylamide-bentonite by phytic acid and its usability in Fe^{3+}, Zn^{2+} and UO_2^{2+} adsorption, Adsorption 9 (2003) 165–175.
[36] A.J. Domb, E.G. Cravalho, R. Langer, The synthesis of poly(hydroxamic acid) from poly(acrylamide), J. Polym. Sci.: Polym. Chem. 26 (1988) 2623–2630.
[37] M. Mullet, P. Fievet, A. Szymczyk, A. Foissy, J.-C. Reggiani, J. Pagetti, A simple and accurate determination of the point of zero charge of seramic membranes, Desalination 121 (1999) 41–48.
[38] H. Lippold, J. Lippmann-Pipke, Effect of humic matter on metal adsorption onto clay materials: testing the linear additive model, J. Contam. Hydrol. 109 (2009) 40–48.
[39] F. Cakicioglu-Ozkan, S. Ulku, The effect of HCl treatment on water vapor adsorption characteristics of clinoptilolite rich natural zeolite, Micropor. Mesopor. Mater. 77 (2005) 47–53.
[40] M. Doğan, M. Alkan, Removal of methyl violet from aqueous solution by perlite, J. Colloid Interface Sci. 267 (2003) 32–41.
[41] W.J. Weber, J.C. Morris, Kinetics of adsorption on carbon from solution, J. Sanit. Eng. Div. Am. Soc. Civ. Eng. 89 (1963) 31–60.
[42] Y.S. Ho, G. McKay, Pseudo-second order model for sorption processes, Process Biochem. 34 (1999) 451–465.
[43] S. Basha, Z.V.P. Murthy, Kinetic and equilibrium models for biosorption of Cr(VI) on chemically modified seaweed, *Cystoseira indica*, Process Biochem. 42 (2007) 1521–1529.
[44] N. Kayaman, E.E.G. Hamurcu, N. Uyanik, M.B. Baysal, Interpenetrating hydrogel networks based on polyacrylamide and poly(itaconic acid): synthesis and characterization, Macromol. Chem. Phys. 200 (1999) 231–238.
[45] D.I. Fortenberry, J.A. Pojman, Solvent-free synthesis of polyacrylamide by frontal polymerization, J. Polym. Sci. Part A: Polym. Chem. 38 (2000) 1129–1135.
[46] T. Perraki, A. Orfanoudaki, Mineralogical study of zeolites from Pentalofos area, Thrace, Greece, Appl. Clay Sci. 25 (2004) 9–16.
[47] C. Covarrubias, R. García, R. Arriagada, J. Yánez, M.T. Garland, Cr(III) exchange on zeolites obtained from kaolin and natural mordenite, Micropor. Mesopor. Mater. 88 (2006) 220–231.
[48] H. Figueiredo, I.C. Neves, C. Quintelas, T. Tavares, M. Taralunga, J. Mijoin, P. Magnoux, Oxidation catalysts prepared from biosorbents supported on zeolites, Appl. Catal. B 66 (2006) 274–280.
[49] M.M.J. Treacy, J.B. Higgins, Collection of Simulated XRD Powder Patterns for Zeolites, fourth revised ed., Elsevier, Amsterdam, 2001.
[50] O. Korkuna, R. Leboda, J. Skubiszewska-Zieba, T. Vrublevs'ka, V.M. Gun'ko, J. Ryczkowski, Structural and physicochemical properties of natural zeolites: clinoptilolite and mordenite, Micropor. Mesopor. Mater. 87 (2006) 243–254.
[51] M.K. Doula, Synthesis of a clinoptilolite–Fe system with high Cu sorption capacity, Chemosphere 67 (2007) 731–740.
[52] J.D. Van Dyke, K.L. Kasperski, Thermogravimetric study of polyacrylamide with evolved gas analysis, J. Polym. Sci. Part A: Polym. Chem. 31 (1993) 1807–1823.
[53] R.T. Yang, Adsorbents: Fundamentals and Applications, John Wıley & Sons, Inc., Canada, 2003.
[54] E. Karadağ, D. Saraydın, O. Güven, Influence of some crosslinker on the swelling of acrylamide–crotonic acid hydrogels, Turk. J. Chem. 21 (1997) 151–161.
[55] D. Xu, C. Chen, X. Tan, J. Hu, X. Wang, Sorption of Th(IV) on Na-rectorite: effect of HA, ionic strength, foreign ions and temperature, Appl. Geochem. 22 (2007) 2892–2906.
[56] P. Rönnback, M. Aström, J. Gustafsson, Comparison of the behaviour of rare earth elements in surface waters, overburden groundwaters and bedrock groundwaters in two granitoidic settings, Eastern Sweden, Appl. Geochem. 23 (2008) 1862–1880.
[57] A.A. Migdisov, A.E. Williams-Jones, T. Wagner, An experimental study of the solubility and speciation of the rare earth elements (III) in fluoride- and chloride-bearing aqueous solutions at temperatures up to 300 °C, Geochim. Cosmochim. Acta 73 (2009) 7087–7109.
[58] C.H. Giles, D. Smith, A. Huitson, A general treatment and classification of the solute adsorption isotherm. I. Theoretical, J. Colloid Interface Sci. 47 (1974) 755–765.
[59] G. Limousin, J.P. Gaudet, L. Charlet, S. Szenknect, V. Barthès, M. Krimissa, Sorption isotherms: a review on physical bases, modeling and measurement, Appl. Geochem. 22 (2007) 249–275.
[60] M.S. Onyango, Y. Kojima, O. Aoyi, E.C. Bernardo, H. Matsuda, Adsorption equilibrium modeling and solution chemistry dependence of fluoride removal from water by trivalent-cation-exchanged zeolite F-9, J. Colloid Interface Sci. 279 (2004) 341–350.
[61] A. Özcan, E.M. Öncü, A.S. Özcan, Kinetics, isotherm and thermodynamic studies of adsorption of Acid Blue 193 from aqueous solutions onto natural sepiolite, Colloids Surf. A 277 (2006) 90–97.
[62] Y. Liu, L. Shen, Langmuir kinetics to first- and second-order rate equations for adsorption, Langmuir 24 (2008) 11625–11630.
[63] K. Dev, R. Pathak, G.N. Rao, Sorption behaviour of lanthanum(III), neodymium(III), terbium(III), thorium(IV) and uranium(VI) on Amberlite XAD-4 resin functionalized with bicine ligands, Talanta 48 (1999) 579–584.
[64] M.M. Saeed, A. Rusheed, Investigation of sorption of Tb(III) by 2-thenoyltrifluoroacetone supported onto polyurethane foam, Radiochim. Acta 90 (2002) 35–42.
[65] Q. Jia, Z.H. Wang, D.Q. Li, C.J. Niu, Adsorption of heavy rare earth(III) with extraction resin containing bis(2,4,4-trimethylpentyl) monothiophosphinic acid, J. Alloys Compd. 374 (2004) 434–437.
[66] B.S. Shaibu, M.L.P. Reddy, D.R. Prabhu, A.S. Kanekar, V.K. Manchanda, N,N′-Dimethyl-N,N′-dibutyl tetradecyl malonamide impregnated magnetic particles for the extraction and separation of radionuclides from nuclear waste streams, Radiochim. Acta 94 (2006) 267–273.
[67] N. Sakamoto, N. Kano, H. Imaizumi, Biosorption of uranium and rare earth elements using biomass of algae, Bioinorg. Chem. Appl. (2008) 1–8.
[68] A. Vlachou, B.D. Symeopoulos, A. Koutinas, A comparative study of neodymium sorption by yeast cells, Radiochim. Acta 97 (2009) 437–441.
[69] Q.H. Fan, M.L. Zhang, Y.Y. Zhang, K.F. Ding, Z.Q. Yang, W.S. Wu, Sorption of Eu(III) and Am(III) on attapulgite: effect of pH, ionic strength and fulvic acid, Radiochim. Acta 98 (2010) 19–25.
[70] An Introduction to Surface Chemistry, Section 2: Adsorption of Molecules on Surfaces, Surface Science Links@Queen Mary, Univ. of London. http://www.chem.qmul.ac.uk/surfaces/scc/scat2.htm (accessed 07.12.10).